J. Physiol. (1980), **308**, *pp.* 217–239
With 6 text-figures
Printed in Great Britain

CONDUCTANCE FLUCTUATIONS FROM THE INACTIVATION PROCESS OF SODIUM CHANNELS IN MYELINATED NERVE FIBRES*

BY F. CONTI†, B. NEUMCKE, W. NONNER‡ AND R. STÄMPFLI

From the I. Physiologisches Institut der Universität des Saarlandes, 6650 Homburg/Saar, Federal Republic of Germany and the †Laboratorio di Cibernetica e Biofisica, CNR, Camogli, Italy

(*Received 30 July 1979*)

SUMMARY

1. Na currents and fluctuations of Na currents were studied under voltage clamp in the same myelinated nerve fibres of *Rana esculenta* at 13 °C. The results were used to test several kinetic models for the gating process of Na channels.

2. Long voltage pulses, depolarizing the membrane by 16–48 mV from a hyperpolarizing holding level of −28 mV, were applied in 4 sec intervals. The d.c. and a.c. components of the membrane current were recorded during the last 328 msec of the 473 msec pulses. For each depolarization, ninety-six trials were made with the node in Ringer solution and, again, after adding 300 nM-tetrodotoxin (TTX) in that solution.

3. The TTX-sensitive d.c. component declined during the 328 msec records by 14–51 % of its time average. The a.c. component was corrected for this trend by subtracting the first from the second of each pair of subsequent records. The TTX-sensitive part of its variance declined, on the average, in parallel to the current, as if the open probability rather than the conductance of the individual Na channels was reduced by a slow process.

4. Single-channel conductances, γ, were calculated on the assumption that Na channels have only one non-zero conductance and were corrected for the limited band width (5 kHz) of the a.c. records. Values of γ increased slightly (< 30 % from 16 to 40 mV), and averaged $8{\cdot}85 \pm 0{\cdot}7$ pS (S.E. of mean, seventeen measurements on ten fibres). This small degree of change in γ suggests that deviations from the all-or-none gating are very small.

5. Power spectral densities of the fluctuations between 3 Hz and 5 kHz were calculated from the trend-free a.c. records and corrected for the TTX-insensitive noise component. Control calculations showed that the only effect of the non-stationarity in the Na current was to enhance the low-frequency points of such spectra by less than 10 %. The spectra revealed at least two Lorentzian components with cut-off frequencies in the range expected from the activation and inactivation kinetics. The low-frequency component became dominant as depolarization was increased.

* Sponsored by Deutsche Forschungsgemeinschaft SFB 38 'Membranforschung'.

‡ Current address: Department of Physiology and Biophysics, University of Washington, SJ-40, Seattle, WA 98195, USA.

0022-3751/80/2290-0421 $07.50

6. Na currents recorded during brief (< 40 msec) depolarizations were analysed in terms of various all-or-none gating models, in which inactivation either was independent of activation (Hodgkin–Huxley (HH) model) or could occur only from the partly or fully activated states (coupled models). The transient Na currents were reproduced by all models.

7. With the parameters from such fits, the fluctuation spectra expected for each model were calculated. The predictions differed in the fraction, r_h, of the variance contributed by the slow (inactivation) fluctuations; r_h was larger in the coupled models than in the HH model.

8. The experimental spectra were divided into two spectral components to yield empirical values for r_h. We used as templates the spectral curves derived for the fast and for the slow fluctuations of the HH model. The empirical r_h values were one (48 mV) to four (16 mV) times larger than those expected for the HH model. They were also larger than the theoretical r_h of the coupled models at the small depolarizations, but became equal or smaller than those at the largest depolarization. Direct comparison of the measured and theoretical spectra revealed the same discrepancies.

9. We conclude that all of the simple gating models considered in this paper are inconsistent with the fluctuation measurements, the coupled models giving slightly smaller deviations than the model with independent activation and inactivation.

INTRODUCTION

Fluctuations of the ionic current reflect properties of individual ionic channels in biological membranes, such as the open-channel conductance and the kinetics of transitions among different channel states (Verveen & De Felice, 1974; Conti & Wanke, 1975; Neher & Stevens, 1977). Their measurement has led to estimates of the conductance of Na and K channels in squid giant axons (Conti, De Felice & Wanke, 1975) and in frog myelinated nerve fibres (Van den Berg, de Goede & Verveen, 1975; Begenisich & Stevens, 1975; Conti, Hille, Neumcke, Nonner & Stämpfli, 1976*a*, *b*; Sigworth, 1977). Comparatively little progress was made, however, towards finding the kinetic scheme that most realistically describes the open-close kinetics of these channels.

The present work investigates in more detail the spectral distribution of the Na current fluctuations in frog nodes of Ranvier. We have extended the previous analysis of Conti *et al.* (1976*a*) down to frequencies of 3 Hz, measuring fluctuations attributable to the inactivation gating. The results are compared with expectations of two different kinds of models, for values of the parameters that fit the macroscopic currents of the same nodes. In the first gating scheme (Hodgkin & Huxley, 1952), the inactivation step is independent of activation, while in the second kind of scheme the two processes are coupled to various degrees (Bezanilla & Armstrong, 1977; Armstrong & Bezanilla, 1977). The models predict low-frequency fluctuations significantly smaller than those observed, the smaller deviation being found with coupled schemes. A preliminary report has been given of part of our results (Conti, Neumcke, Nonner & Stämpfli, 1979).

METHODS

Measurements

The experimental procedure was developed from that of Conti *et al.* (1976*a*). Major improvements were an on-line-computer acquisition of macroscopic voltage-clamp currents, a measurement of the time course of the variance of the current fluctuations, and a particular procedure to avoid low-frequency artifacts in the spectral densities due to systematic slow drifts in the currents.

Single fibres were dissected from the tibial nerve of *Rana esculenta* (Stämpfli, 1969) and studied under voltage-clamp conditions by the method of Nonner (1969). A short voltage-measuring internode, with air-gap insulation, and a long current-injecting internode were used as in Conti *et al.* (1976*a*). All measurements were made at 13 °C on nodes bathed in a continuously flowing solution containing: 105 mM-NaCl, 2 mM-$CaCl_2$, 10 mM-tetraethylammonium (TEA) chloride and 2 mM-morpholinopropanesulphonic acid-NaOH buffer at pH 7·4. For control measurements, 300 nM-TTX was added to the perfusion fluid. The 'artificial axoplasm' contained 113 mM-CsCl and 7 mM-NaCl. In these conditions, there was no significant current from K channels. The zero-current level of the membrane potential was taken as that corresponding to 30 % Na current inactivation; for calculations of permeabilities, the absolute membrane potential at this level was assumed to be − 70 mV. The membrane potentials are given in this paper as the depolarizations from the zero-current level. Except for two fibres dissected from a motor bundle, the fibres were sensory and gave repetitive action potentials with long stimuli. In all nodes the first action potential was close to 120 mV in amplitude.

Macroscopic currents. During the first 10 min of each experiment the macroscopic current relaxations following steps of membrane potential were studied. The currents were recorded at a band width of 25 kHz, after analog subtraction of most of the leakage and capacitive components (simulated by the super-position of three different exponential currents plus a d.c. step). The amplifier of the current signal had a variable gain selected by the computer. Forty-one different sequences of voltage pulses, generated by the computer through a 13-bit, digital-to-analog (D/A) converter, were applied in programmed succession to the node. They were applied from a holding potential of − 28 mV, and each sequence consisted of a prepulse and a test pulse, followed by two similar combinations of pulses with opposite polarity and half amplitude. The sum of the currents measured in the three successive pulse combinations was taken as the current carried by Na channels. Pulse sequences yielding small Na currents were repeated 2 to 16 times and averaged for a larger signal-to-noise ratio.

Steady-state currents. The steady-state current during the fluctuation measurements must be known for estimates of the single-channel conductance. During each depolarization from the holding potential of − 28 mV, this current was measured at a relatively low gain and through a low-pass filter with 100 Hz cut-off frequency. Uncompensated linear components were eliminated by adding the response to a hyperpolarizing step of the same amplitude, measured once after every six consecutive depolarizations. The record was digitally filtered by condensation of each 128 consecutive points and yielded thirty-two values at about 10 msec intervals. In measurements with TTX the above procedure gave average currents that were less than 1 % of those obtained without TTX. As a rule, the current declined significantly (up to 40 %) from the beginning to the end of each fluctuation record, which started 145 msec after the onset of the test depolarization and had a duration, T, of 328 msec.

Current fluctuations. In preliminary experiments and in our previous study (Conti *et al.* 1976*a*, *b*), the slow variation of the Na current during the step depolarization was found to obscure the measurements of slow fluctuations attributable to the inactivation process. Removing the slow systematic drift from the a.c. signal before the spectral analysis reduced the power density at low frequencies by one to two orders of magnitude. The drift of the a.c. signal was carefully eliminated as follows. First of all, the fluctuation measurement was started no earlier than 145 msec after the onset of the pulse. The d.c. component and slow drift of the a.c. signal were approximately compensated by an analog circuit. This circuit stored the current signal present at 145 msec by charging a capacitor; between 145 and 473 msec (when fluctuations were recorded), a small adjustable current was supplied to the capacitor for simulating the drift, and the voltage across the capacitor was continuously subtracted from the a.c. signal. The circuit

was adjusted during a few test sweeps before the recorded measurements. This raw, analog subtraction was made exact by subtracting the first from the second of each pair of digital fluctuation records. The digital subtraction was essential, although (as explained later) it doubled the number of records required for a given accuracy in the spectral points. The a.c. signal was filtered through an 8-pole Butterworth low-pass at 5 kHz. The gain of the a.c. preamplifier was under control of the computer; with the analog subtraction of d.c. and drift, the gain could be optimally chosen, such that the root mean square (r.m.s.) value of the recorded signal was just smaller than $\frac{1}{8}$ of the dynamic range of the A/D converter.

Each noise record consisted of 4096 twelve-bit samples at 80 μsec intervals. From difference records, power density spectra were calculated on-line by the Fast Fourier Transform without multiplying by any time window function, and spectral points were condensed at high frequencies as in Conti *et al.* (1976*a*). The reliable frequency range of the spectra was 3·05–5000 Hz. In each experimental condition we measured the spectra from 48 pairs of trials, taken in a period of about 7 min. In the off-line analysis, filter attenuations up to 5 kHz were corrected and the average spectral densities over all trials were calculated.

The time course of the variance was also measured from the same records. The time average of the a.c. signal, obtained from the block of 4096 samples, was first subtracted from each point. This difference was squared, averaged in blocks of 128 consecutive points and divided by two, to yield the average variance in intervals of *ca.* 10 msec. Each difference record yielded thirty-two variance points, which were then ensemble averaged over all forty-eight trials. Since each record was at least sixty times longer than the effective correlation time of our fluctuations, any systematic underestimation of the variance should have been less than 3 %.

Fluctuation measurements were taken in each fibre at two different membrane potentials and then repeated in TTX Ringer. Power spectra and variances for test and TTX Ringer were subtracted. Except for depolarizations of 8 mV, the subtraction of control noise did not decrease significantly the accuracy of the final results. The relaxation and fluctuation measurements at two different potentials in test and TTX Ringer took altogether about 40 min.

Errors of power spectra

Our measurements of power spectra, from averages over ensembles of difference records of finite duration, are subject both to systematic and to random errors. The random errors were estimated as the standard deviations of the measured spectral densities. The standard deviation of the power contained in the frequency interval β will generally decrease as $1/\sqrt{N\beta T}$ (Rice, 1944) where N is the number of records averaged. Indeed, the relative error in our spectra was about 15 % for the low-frequency points (up to 66 Hz) and decreased upon increasing the number of points condensed to 1·5 % at the highest frequencies.

Systematic errors arise both from the limited duration of the records and from possible non-stationarities reflected by the drifts in the mean current already mentioned. These errors affect the expectation value of the measured spectra. To evaluate them, let $X(t)$ be the stochastic variable observed from $t = 0$ to $t = T$ in $2N$ successive and independent trials, let $\xi^{(j)}(t)$ be the particular realization of $X(t)$ in the jth trial, and

$$\delta\xi^{(j)}(t) = \xi^{(j)}(t) - \langle X(t)\rangle$$

where the brackets, $\langle\ \rangle$, denote the expectation. It is convenient to elaborate our considerations in terms of autocorrelation functions rather than power spectra. The Wiener–Khintchin theorem (Lee, 1960) assures us that the two treatments are equivalent. The experimental procedure described above would measure the empirical auto-covariance of X

$$C_{\text{emp}}(\tau) = \frac{1}{2N}\sum_{j=1}^{N} \mathrm{R}_{\mathrm{T}}\{\delta\xi^{(2j-1)}(t) - \delta\xi^{(2j)}(t);\tau\}, \tag{1}$$

where, due to the limited duration of our records, the sum implies the truncated autocorrelation function, R_{T}, defined by

$$R_{\mathrm{T}}\{y(t);\tau\} = \frac{1}{\mathrm{T}}\left\{\int_0^{T-\tau} y(t)y(t+\tau)dt + \int_0^{\tau} y(t)y(t+T-\tau)dt\right\}. \tag{2}$$

The function $R_\tau\{\delta\xi^{(2j-1)}(t) - \delta\xi^{(2j)}(t);\tau\}$ can be split into four terms, two of which represent the truncated autocorrelation functions of $\delta\xi^{(2j-1)}(t)$ and of $\delta\xi^{(2j)}(t)$ and the other two represent their cross-correlations functions. Since the integral and the expectation operators commute (Soong, 1973) and since $\xi^{(2j-1)}(t)$ and $\xi^{(2j)}(t)$ are independent realizations of the stochastic variable, it is easily seen that the cross-correlation terms have zero expectation value and eqn. (1) yields

$$\langle C_{\text{emp}}(\tau)\rangle = \frac{1}{T}\left\{\int_0^{T-\tau} C(t, t+\tau)\mathrm{d}t + \int_0^{\tau} C(t, t+T-\tau)\mathrm{d}t\right\}, \tag{3}$$

where $C(t, t+\tau)$ is the true autocovariance of $X(t)$:

$$C(t, t+\tau) = \langle (X(t) - \langle X(t)\rangle)\,(X(t+\tau) - \langle X(t+\tau)\rangle)\rangle. \tag{4}$$

If $X(t)$ is stationary,

$$C(t, t+\tau) = C(\tau) = \langle (X(0) - \langle X\rangle)\,(X(t) - \langle X\rangle)\rangle, \tag{5}$$

and eqn. (3) reduces to

$$\langle C_{\text{emp}}(\tau)\rangle = \frac{1}{T}\{(T-\tau)\,C(\tau) + \tau C(T-\tau)\}. \tag{6}$$

Eqns. (3) and (6) provide the basis for estimating systematic errors in our measurements.

For stationary fluctuations with $C(\tau)$ given by the sum of a finite number of exponentials, the error due to truncation is largest in the component with the slowest relaxation. This component has a relaxation time, τ_h, smaller than 10 msec (see Table 1 for $V \geqslant 16$ mV). In our measurements, $T \sim 328$ msec, and eqn. (6) shows that the systematic error in the measurement of the slowest component of $C(\tau)$ is, therefore, less than 3%. Taking the Fourier transform of eqn. (6) to obtain a relationship involving power spectra, one can show that the above error affects each point of the Lorentzian spectrum corresponding to the slowest relaxation by less than 3%. Systematic errors due to very slow relaxations (with time constants of the order of T) will be evaluated in Results, again on the basis of eqn. (3).

A more complicated argument, involving the estimate of the variance of integrals of stochastic variables (Soong, 1973), would show that the four terms contained in $R_T\{\delta\xi^{(2j-1)}(t) - \delta\xi^{(2j)}(t), \tau\}$ all have the same variance. Thus, as already mentioned, the random error of averages from N difference records (derived from $2N$ independent trials) is equal to the error of averages from N individual records. The advantage of the difference method consists in the elimination of the expectation value, $\langle X(t)\rangle$, without need of measuring it. By analyzing directly the individual records we would have obtained estimates of autocorrelation functions containing the additional systematic contribution of the autocorrelation of $\langle X(t)\rangle$. As we verified in preliminary experiments, this contribution was very large and not subject to any reliable correction *a posteriori*.

Off-line analysis of the macroscopic currents

The theoretical background for calculating the time course of macroscopic current relaxations and the properties of stationary current fluctuations for a general, n-state gating process is well established (see Conti & Wanke, 1975; Neher & Stevens, 1977; Colquhoun & Hawkes, 1977). This last section of the Methods is therefore confined to presenting the various kinetic schemes to be studied and to describing the practical procedure of finding their parameters from the macroscopic current measurements. The method of evaluation used for the spectra will be described in Results.

We started from an analysis in terms of the Hodgkin-Huxley equations (Hodgkin & Huxley, 1952). Measurements of Na peak currents for 60 mV depolarizations following long prepulses in the range -48 mV to $+48$ mV yielded the inactivation curve $h_\infty(V)$. The next seven records, with prepulses to $V = +8$ mV of different durations followed by test pulses to $+60$ mV, provided a measurement of τ_h at $+8$ mV. Two similar series were used to evaluate τ_h for the two membrane

potentials, V_A and V_B, at which later measurements of fluctuations were performed. The reversal potential, V_{Na}, was measured from the peak responses to six depolarizations ranging from +60 to +144 mV. These depolarizations were preceded by 100 msec prepulses to +8 mV, which reduced the amplitude of the currents and thus minimized series-resistance artifacts. The same responses were used to estimate the current, $I_{max}(V)$, that would flow if all channels were open. Following Dodge & Frankenhaeuser (1959), we assumed that $I_{max}(V)$ obeyed the constant field equation. Then,

$$I_{max}(V) = G_{max}(V-70)\frac{1-\exp\{(V-V_{Na})/24{\cdot}7\}}{1-\exp\{(V-70)/24{\cdot}7\}} = G_{max}\,f(V), \tag{7}$$

where V and V_{Na} are in units of mV, and G_{max} is a conductance. G_{max} was measured as the asymptotic value, for large depolarizations, of $I_0(V)/h_0 f(V)$, where $I_0(V)$ was found by extrapolating the time course of Na current inactivation to the onset of the test depolarization and h_0 gives the steady-state inactivation at the end of the +8 mV prepulse. The final three records provided the currents for steps from −28 to +8 mV and from +8 mV to V_A and V_B. They yielded m_∞, τ_m and a further estimate of τ_h at these depolarizations. $m_\infty(V)$ was measured as $\{I_0(V)/h_0 I_{max}(V)\}^{1/3}$; $\tau_m(V)$ and $\tau_h(V)$ were obtained from computer fits of the time course of the voltage-clamp currents, with the m_∞ and h_∞ values already determined.

A similar analysis of the macroscopic currents was repeated for each of the other kinetic schemes considered, in which activation and inactivation were coupled. These schemes, as well as the HH model, can be described as particular cases of the general diagram:

$$\begin{array}{ccccccc}
 & & 3\alpha q'' & & 2\alpha q' & & \alpha q \\
[1'] & \rightleftharpoons & [2'] & \rightleftharpoons & [3'] & \rightleftharpoons & [4'] \\
 & & \beta q'' & & 2\beta q' & & 3\beta q \\
\kappa q'' \Big\downarrow \uparrow \lambda q'' & & \kappa q' \Big\downarrow \uparrow \lambda q' & & \kappa q \Big\downarrow \uparrow \lambda q & & \kappa \Big\downarrow \uparrow \lambda \\
 & & 3\alpha & & 2\alpha & & \alpha \\
[1] & \rightleftharpoons & [2] & \rightleftharpoons & [3] & \rightleftharpoons & [4] \\
 & & \beta & & 2\beta & & 3\beta
\end{array}, \tag{A}$$

where state [4] represents the open channel and is the only state with non-zero conductance. For $q = q' = q'' = 1$, $\kappa = \beta_h$, $\lambda = \alpha_h$, scheme (*A*) reduces to the HH scheme, in which transitions to primed (inactivated) states can occur from any non-primed state with the same probability. In the coupled diagrams considered in this paper, $q'' = q' = 0$; that is, the chain of steps leading to the opening of the channels is the same as in the HH scheme, but inactivation can only occur at an advanced stage of activation, from the last closed state [3] or from the open state [4]. These schemes are close to that proposed by Armstrong & Bezanilla (1977) to account for partial immobilization of gating charges in squid giant axons during inactivation, but they imply that the rate constants of the activation steps have the same ratios as those of the HH scheme.

The first steps in the fit of a coupled scheme were the same as for the HH scheme. The probability of occupation of states [3'] and [4'] was numerically equal to the HH inactivation, $1-h_\infty$. Likewise, the estimates of $I_0(V)$ from the HH scheme were maintained as a first approximation (and upper limit) to the sodium current that would flow in the absence of inactivation. A first, tentative set of parameters for 8 mV, V_A, and V_B was obtained by varying the ratios κ/λ and β/α in order to get adequate equilibrium probabilities for the inactivated states and for the open state. κ and λ were then both multiplied by a suitable common factor to fit the time course of the late decay of the currents, and β and α were varied by a common factor to fit the initial rise of the currents. Final adjustments were made by allowing small variations of κ/λ, β/α and $I_0(V)$ in order to fit the ratio of peak to steady-state currents. These fits were all judged by eye from an oscilloscope display of measured and theoretical curves. Since the number of free parameters in these models was no larger than in the HH model, these parameters could also be optimized within narrow limits.

We also made an attempt to fit the current relaxations with a strictly sequential scheme similar to that discussed by Bezanilla & Armstrong (1977) (scheme (A) with $q = q' = q'' = 0$). We had to discard the scheme at this stage, since it did not yield acceptable fits of the macroscopic currents.

RESULTS

Transient Na currents

A full analysis of voltage-clamp currents according to the HH scheme or according to the coupled scheme with $q = 0{\cdot}5$, $q = 1$, or $q = 5$ was performed on six different nodes. The values of the kinetic parameters are given in Tables 1 and 2. It is seen

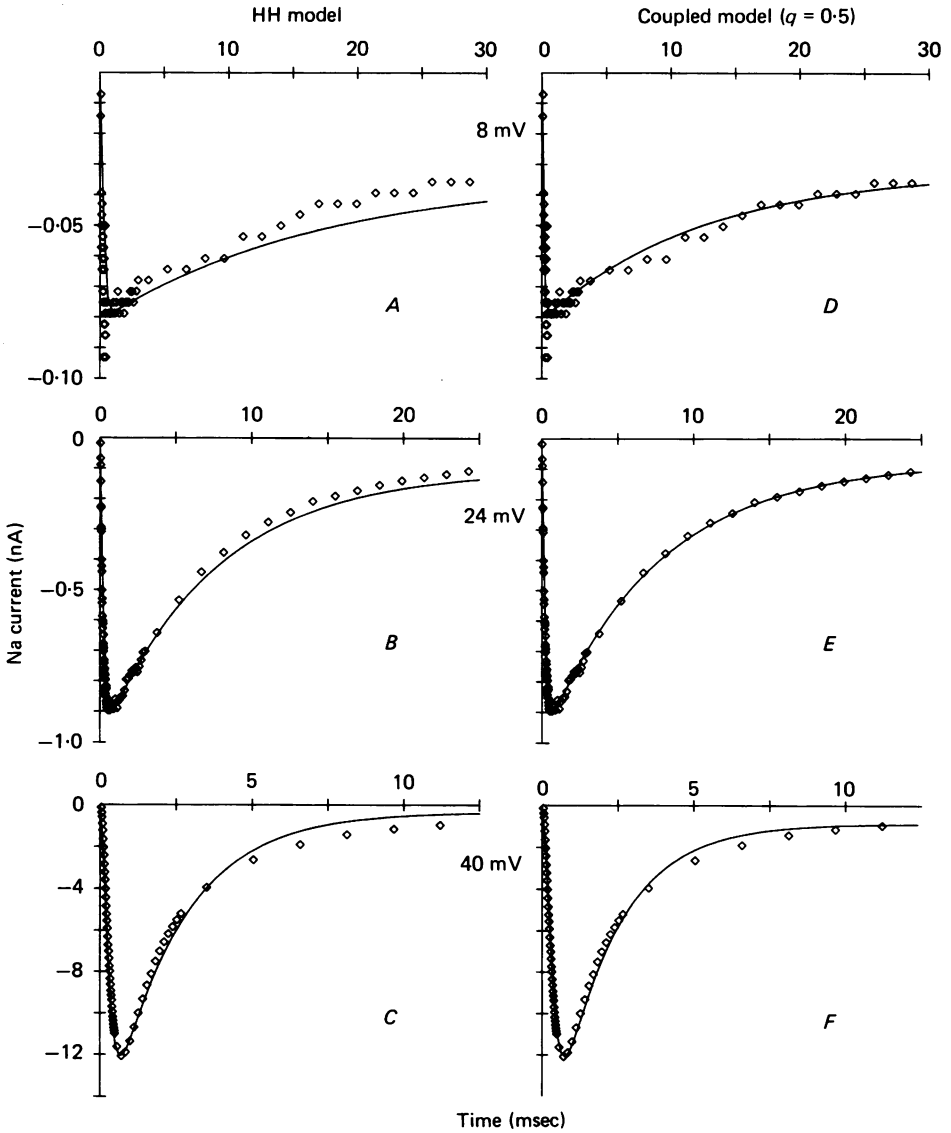

Fig. 1. Fit of transient Na currents for the HH kinetic scheme (*A–C*) and the coupled scheme with $q' = q'' = 0$, $q = 0{\cdot}5$ (*D–F*). Points represent Na current and have been corrected for leakage and capacity current as described in Methods; *K* current was blocked by external TEA and internal Cs ion; 13 °C. Test pulses to 24 and 40 mV were preceded by 100 msec depolarizing prepulses to + 8 mV; the test pulse to + 8 mV was applied from the hyperpolarizing holding potential (− 28 mV). Parameters of currents are given in Tables 1 and 2 (node 12); in the fits *A–C*, h_∞ was fixed to the values obtained from double-pulse measurements.

from Table 1 that the estimate of τ_h from the decline of the voltage-clamp current during the test pulse (τ_h'') was in general slightly higher than that obtained from double-pulse experiments $(\tau)_h'$, but the difference never exceeded 30 %. The variation in the estimates of the other HH parameters among nodes never exceeded 50 %, and probably were due to a difference of a few millivolts in the adjustment of the zero-current potential. Such small voltage displacements were revealed by the comparison of $h_\infty(V)$ curves from different nodes. A good reproducibility of the parameters was obtained also with the coupled schemes (Table 2). Fig. 1 shows examples of the fit with the HH scheme (A, B, C) and with the coupled scheme with $q' = q'' = 0$ and $q = 0{\cdot}5$ (D, E, F). All records are from the same node. Both schemes give a rather poor fit of the late decay of the Na currents, which could be better described by two exponentials (Chiu, 1977; Nonner, 1980). However, describing inactivation itself as a second-order process would have complicated our analysis considerably and was reserved for future work.

TABLE 1. Parameters of transient Na currents: Hodgkin–Huxley model

Node	V (mV)	h_∞	τ_h' (msec)	τ_h'' (msec)	m_∞	τ_m (μsec)
8	8	0·31	10·7	12·4	0·10	—
9	8	0·37	10·5	11·3	0·09	—
10	8	0·34	11·2	14·7	0·10	—
11	8	0·32	11·1	12·6	0·10	77
12	8	0·42	11·1	17·3	0·084	168
13	8	0·30	10·5	10·6	0·13	—
Mean	8	0·34	10·9	13·2	0·10	123
8	16	0·098	8·7	9·4	0·17	93
9	16	0·144	9·3	9·2	0·16	82
13	16	0·097	9·5	9·3	0·20	54
Mean	16	0·110	9·2	9·3	0·18	76
11	24	0·031	6·5	7·2	0·32	178
12	24	0·043	8·2	7·4	0·28	161
Mean	24	0·037	7·4	7·3	0·30	170
8	32	0·012	4·1	5·2	0·50	175
10	32	0·012	2·8	3·15	0·57	214
13	32	0·012	2·5	3·6	0·59	189
Mean	32	0·012	3·1	4·0	0·55	193
9	40	0·014	2·6	2·75	0·68	148
12	40	0·008	1·9	1·8	0·77	155
Mean	40	0·011	2·3	2·3	0·73	152
10	48	0·004	—	1·35	0·84	116

Inactivation time constants were determined with the double-pulse method (τ_h') and from the decline of the Na current during a test depolarization (τ_h''). The mean values of h_∞, m_∞, and τ_h for $V = 16$, 24, 32, and 40 mV were used in the fit of spectra from four other nodes, for which the full analysis of the transient currents was not performed.

Variance of the fluctuations and single-channel conductance

Since two different kinds of information can be derived from fluctuation measurements, we divided the analysis into two parts. First, the variance of the fluctuations was used to study the stationarity of the underlying stochastic process and to obtain estimates of single-channel conductance. Then the spectral distribution of the

TABLE 2. Parameters of transient Na currents: three coupled models

		$q = 0{\cdot}5$				$q = 1$				$q = 5$			
Node	V(mV)	α (msec^{-1})	β (msec^{-1})	κ (msec^{-1})	$\lambda(10^{-3}$ msec^{-1})	α (msec^{-1})	β (msec^{-1})	κ (msec^{-1})	$\lambda(10^{-3}$ msec^{-1})	α (msec^{-1})	β (msec^{-1})	κ (msec^{-1})	$\lambda(10^{-3}$ msec^{-1})
8	8	1·0	7·2	4·2	50	1·00	7·7	2·1	27	1·0	7·7	0·42	5·4
9	8	1·0	8·1	4·6	50	0·98	8·4	2·3	30	1·0	8·7	0·46	5·5
10	8	0·95	7·3	3·5	35	0·95	7·4	2·0	23	0·95	7·7	0·40	4·6
11	8	1·0	7·6	4·0	45	1·00	8·0	2·0	25	1·0	8·2	0·40	5·0
12	8	1·14	10·6	4·6	54	0·95	8·9	2·3	27	1·1	11·0	0·46	5·4
13	8	1·2	6·6	3·4	50	1·20	6·8	1·8	29	1·2	7·1	0·36	5·8
Mean	8	1·05	7·9	4·05	47	1·01	7·9	2·1	27	1·0	8·4	0·42	5·3
8	16	1·6	5·5	1·7	8	1·6	6·0	1·1	7	1·6	6·0	0·22	1·1
9	16	1·8	6·5	1·7	9	1·8	7·2	1·1	8	1·8	7·2	0·22	1·3
13	16	2·0	5·7	1·3	6	2·0	6·0	0·85	5·5	2·0	6·2	0·17	0·9
Mean	16	1·8	5·9	1·6	7·7	1·8	6·4	1·0	6·8	1·8	6·5	0·20	1·1
11	24	2·7	4·6	0·8	5·0	2·6	4·7	0·55	4·3	2·6	4·9	0·12	0·8
12	24	2·3	4·7	1·0	5·4	2·3	4·9	0·55	3	2·3	5·0	0·13	0·6
Mean	24	2·5	4·65	0·9	5·2	2·45	4·8	0·55	3·7	2·5	4·95	0·125	0·7
8	32	4·0	2·7	0·5	5·4	4·0	3·0	0·32	2·7	4·0	3·1	0·09	1·2
10	32	4·4	2·3	0·55	5·0	4·4	2·6	0·40	3·8	4·4	2·8	0·11	1·0
13	32	4·6	1·6	0·5	4·5	4·6	1·9	0·39	4·7	4·6	2·1	0·10	1·0
Mean	32	4·3	2·2	0·52	5·0	4·3	2·5	0·37	3·7	4·3	2·7	0·10	1·1
9	40	6·6	1·3	0·5	7	6·2	1·8	0·39	5·5	6·2	1·6	0·15	2·0
12	40	5·0	0·6	0·8	12	5·5	0·8	0·60	5	5·5	0·6	0·35	4·0
Mean	40	5·8	0·95	0·65	9·5	5·9	1·3	0·50	5·3	5·9	1·1	0·25	3·0
10	48	12	0·4	0·8	4·0	8·2	0·6	0·70	4	8·2	0·4	0·45	2·0

All models are represented by the kinetic scheme (A) where $q' = q'' = 0$ and q as indicated.

fluctuations was analyzed in terms of normalized power spectral densities. With the normalization chosen, the spectra depended only on the kinetics of the fluctuations and were directly comparable from node to node.

The time course of the variance of current fluctuations during step depolarizations was measured from difference records as described in Methods. The reason to measure the variance as a function of time was the observation of systematic drifts in the current, which suggested that the Na current had not reached a true steady state even after 500 msec. Fig. 2 illustrates the variety of results obtained in different

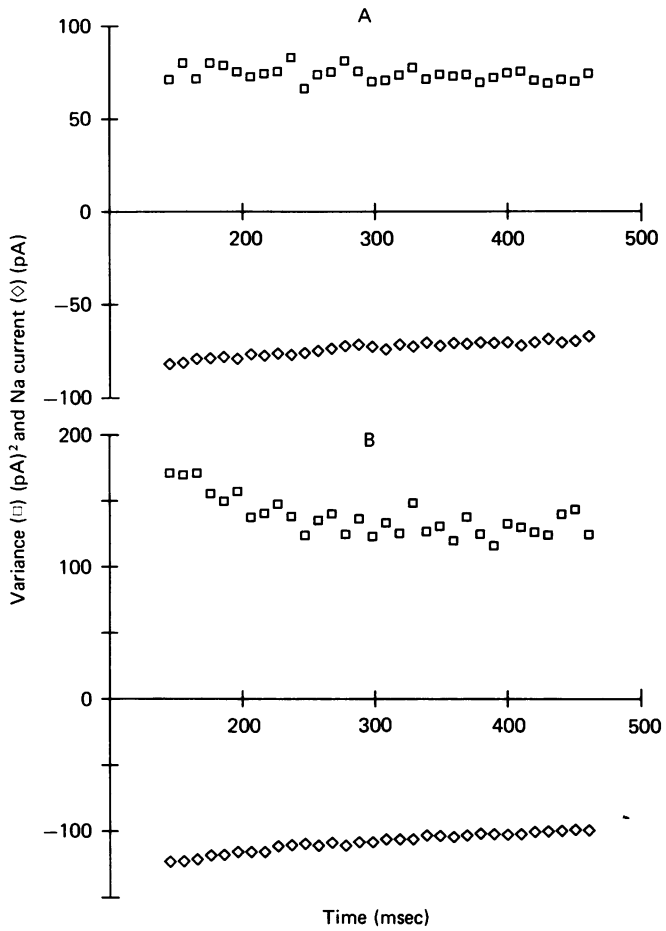

Fig. 2. Time course of the mean Na current, I, and of the variance of Na current fluctuations, σ^2, during long depolarizations of +24 mV in two different nodes. *A*, node 12; *B*, node 5. Ensemble averages over forty-eight pairs of successive trials, obtained as described in Methods. TTX-insensitive components have been subtracted. Fluctuations were measured with 5 kHz band width.

experiments, showing the Na current and its variance between 145 and 473 msec of step depolarizations to 24 mV. In the experiment of Fig. 2*A* the Na current decreased monotonously by 17 % in these 328 msec, while there was a much smaller decrease (~3 %) in the variance over the same period. Fig. 2*B* shows the results from another node. Here both the current and the variance declined in a more similar way, by 18

and 27 %. On the average of all nodes, the current and the variance were found to fall almost in parallel (Table 3). The decline was strongest with the largest depolarization and was insignificant in the control measurements with TTX. It probably arose from a slow inactivation of the sodium channels (Adelman & Palti, 1969; Peganov, Khodorov & Shishkova, 1973).

TABLE 3. Na current and its fluctuation variance: slow changes during depolarization

Node	V (mV)	$\bar{I}$ (pA)	$\frac{\Delta I}{\bar{I}}$	$\overline{\sigma^2}$ (pA²)	$\frac{\Delta\sigma^2}{\overline{\sigma^2}}$
4	16	−61	0·20	39	0·15
8	16	−40	0·076	25	0·32
9	16	−59	0·15	46	0·33
13	16	−43	0·12	37	0·0
Mean	16	−50·5	0·14	37	0·20
4	24	−81	0·31	70	0·19
5	24	−109	0·20	138	0·33
6	24	−129	0·25	96	0·36
11	24	−71	0·34	57	0·28
12	24	−74	0·19	74	0·027
Mean	24	−93	0·26	87	0·24
3	32	−107	0·27	117	0·26
8	32	−54	0·46	70	0·36
10	32	−86	0·27	82	0·37
13	32	−80	0·10	63	0·16
Mean	32	−82	0·28	83	0·29
6	40	−175	0·63	221	0·79
9	40	−131	0·50	143	0·66
12	40	−110	0·41	124	0·33
Mean	40	−139	0·51	163	0·60
10	48	−67	0·38	83	0·34

The changes with time of Na current, ΔI, and of fluctuation variance, $\Delta\sigma^2$, are the difference of the values at 145 and at 473 msec after the onset of the step depolarization. $\bar{I}$ and $\overline{\sigma^2}$ are the average values during that interval.

If Na channels can assume only one level of non-zero conductance, a parallel variation with time of the Na current and the variance indicates that the slow inactivation process does not affect this open-channel conductance. The assumption of a unique non-zero conductance, which is supported by previous fluctuation analysis (Conti *et al.* 1976*b*; Sigworth, 1977), is made in all models considered in this work. It implies that (Neher & Stevens, 1977)

$$\sigma^2 = Ni^2 p(1-p) = Ii(1-p) \tag{8}$$

where I is the Na current of the node, σ^2 is its variance, i is the current flowing through a single open channel, and p is the probability that the channel is open ($p \ll 1$ in all of our measurements). Hence changes in I due to changes of p would yield equal relative changes of σ^2, like those observed. On the other hand, changes in i would yield larger percentage changes in σ^2, contrary to what is observed.

If $p \ll 1$, eqn. (8) simplifies to

$$i = \frac{\sigma^2}{I} \tag{9}$$

In our analysis, we inserted for I the time average of the mean current, $\bar{I}$, and for the variance, $b\overline{\sigma^2}$, where $\overline{\sigma^2}$ was the time average of the observed variance, obtained from results as in Fig. 2. The factor b (Table 4) corrected this empirical variance for the limited band width of the measurements and was derived from the analysis of the spectra described later. The single-channel currents were then converted into the single-channel chord conductances, γ, for $V = 70$ mV, under the assumption that the instantaneous i–V curve for Na channels is described by the constant-field equation.

TABLE 4. Analysis of the Na current fluctuations

Node	V (mV)	τ_m (μsec)	b	$-i$ (pA)	γ (pS)
4	16	112	1·54	1·0	5·4
8	16	90	1·70	1·08	5·7
9	16	74	1·93	1·5	7·6
13	16	42	2·66	2·27	12·3
Mean	16	80	1·96	1·46	7·8
4	24	189	1·22	1·06	6·4
5	24	198	1·20	1·52	9·0
6	24	121	1·36	1·01	6·1
11	24	140	1·31	1·04	6·3
12	24	113	1·41	1·42	8·0
Mean	24	152	1·30	1·21	7·2
3	32	84	1·35	1·48	10·0
8	32	108	1·25	1·62	10·8
10	32	110	1·18	1·13	8·7
13	32	145	1·16	0·92	6·3
Mean	32	112	1·24	1·29	9·0
6	40	85	1·19	1·5	11·6
9	40	75	1·24	1·35	9·9
12	40	59	1·29	1·45	10·6
Mean	40	73	1·24	1·44	10·7
10	48	40	1·24	1·55	15·7
Overall mean (± S.E. of mean)					8·55 (±0·7)

τ_m and b were found from the fit of spectra with eqn. (18). i was calculated from eqn. (9) with $I = \bar{I}$ and $\sigma^2 = b\overline{\sigma^2}$ (for $\bar{I}$, $\overline{\sigma^2}$ see Table 3), γ is a chord conductance normalized to 70 mV depolarization (Conti *et al.* 1976*a*).

The results of the analysis are given in Table 4. The average single-channel conductance obtained from our present data is 8·85 pS. This value is in good agreement with those obtained by Conti *et al.* (1976*a*) from the analysis of stationary high-frequency fluctuations, and by Sigworth (1977) from the analysis of Na current fluctuations during the early, transient phase. The agreement reinforces the idea that the inactivation of Na channels is all-or-nothing. For example, if the inactivated channel had even only 1 % of the conductance of the open channel, then the single-channel conductance estimated by us during long depolarizations with $h_\infty = 0{\cdot}01$ ($V = 40$ mV) would be less than half of that estimated by Sigworth in the early phase of the response, when $h \simeq 1$.

Channels with two states of non-zero conductance carry the macroscopic current

$$I = N(p_1 i_1 + p_2 i_2) \tag{10}$$

that fluctuates with a variance

$$\sigma^2 = N\{p_1 i_1^2 + p_2 i_2^2 - (p_1 i_1 + p_2 i_2)^2\}, \quad (11)$$

where p_1, p_2 are the probabilities, and i_1, i_2 the single-channel currents, for the fully open and inactivated states ($i_2 = 0{\cdot}01\ i_1$ in our example). In the absence of inactivation ($p_2 = 0$), the quotient $\sigma^2/\{I(1-p_1)\}$ would yield i_1. When 99% of the channels are inactivated ($p_2 = 0{\cdot}99$), the quotient σ^2/I would represent currents between $\sim i_1/2$ (with the rest of the channels fully open, $p_1 = 0{\cdot}01$) and $i_2 = i_1/100$ (with the rest of the channels closed, $p_1 = 0$).

Table 4 shows a tendency for the γ estimates to increase for increasing depolarizations. This effect was also present in the data of Conti *et al.* (1976*a*) and Sigworth (1979). If we disregard the single experiment at $V = 48$ mV, which is likely to be affected by the largest errors from the run-down of the fibre, the voltage dependence of the conductances in Table 4 could be explained by a very small, residual conductance in non-activated channels. However, the phenomenon could also arise from an improper correction for the limited band width. The correction factor, b, was largest at 16 mV and thus may have particularly biased the values of γ measured with that voltage step.

Spectral distribution of current fluctuations

The spectral distributions of Na current fluctuations at five different potentials are shown in Fig. 3. The points were obtained by subtracting spectral densities in TTX Ringer from those in test Ringer and dividing the result by the difference of the measured variances, corrected for a band width factor estimated as described below. These power spectral densities are in units of Hz^{-1} and have been scaled in such a way that the integral of their theoretical fit over all positive frequencies is unity. Comparing the results of measurements from different fibres at the same membrane potential showed that the scatter among them was of the same order as the scatter of the points in each spectrum. This confirmed the reproducibility of the normalized spectra, which should be independent of errors in the current calibration, of the nodal area, and of factors affecting the single-channel current or the number of excitable channels, such as the reversal potential of the Na current or long-term inactivation. The spectra of Fig. 3 are similar to those reported by Conti *et al.* (1976*a*) for frequencies above 100 Hz, but they add new information in the range of 3–100 Hz, where they show a fair tendency to reach a low-frequency plateau. Comparison with straight lines with slope -1, drawn in the Fig. 3*A*, *B* and representing $1/f$ characteristics (Verveen & De Felice, 1974), shows that major contributions from this kind of noise were absent in our present measurements. Indeed fairly good fits of the data were obtained, as described later, with theoretical curves that contained no $1/f$ component. A small excess noise above these theoretical curves was sometimes seen at the low-frequency end of the spectrum (Fig. 3*D*, *E*), but, as explained below, this could be caused by a non-stationarity of the fluctuations. The absence of $1/f$ noise reported here may appear to be in contrast with the results of previous measurements (Conti *et al.* 1976*a*, *b*). However, it had already been stressed by these authors that their low-frequency points probably were not reliable. The new results confirm the suspicion of Conti *et al.* that their spectral densities for frequencies below 300 Hz were

artifactually enhanced by trends in the a.c. signal, which have been eliminated with the present technique.

Effects of slow non-stationarities

The time dependence of the variance in Fig. 2 shows that the measured fluctuations are not completely stationary, and the question arises of how much this could affect our spectral measurements.

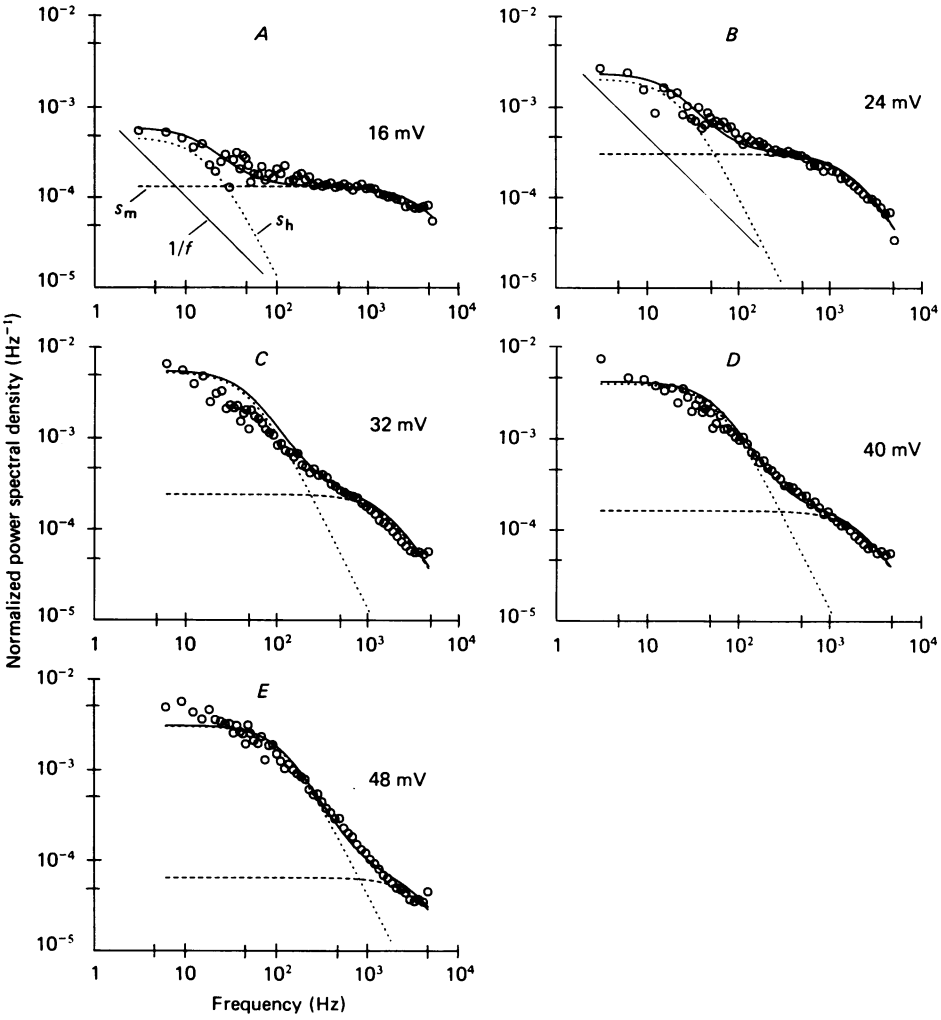

Fig. 3. Na current fluctuation spectra at five potentials. The normalized power density spectra, $S/b\overline{\sigma^2}$, were taken from three fibres: 9 (*A*, *D*), 11 (*B*), 10 (*C*, *E*). The power spectral density, S, and the variance $\overline{\sigma^2}$ were obtained by subtracting the values measured in TTX Ringer from those in test Ringer. The band width correction factors, b, are given in Table 4. Continuous curves represent fitted spectra, $s(f)$, defined by eqns. (18)–(20). For comparison, the components $r_h s_h$ (dotted line) and $(1\text{-}r_h)s_m$ (dashed line) are also shown. The straight lines with slope -1 in *A* and *B* are drawn in order to emphasize the absence of a significant $1/f$ component.

First of all, we verified that the fraction of the variance attributable to inactivation gating (column r_h in Table 5) was independent of the relative change of the variance during the depolarization (column $\Delta\sigma^2/\overline{\sigma^2}$ in Table 3). Obviously there is no correlation between the values of $\Delta\sigma^2/\overline{\sigma^2}$ and r_h obtained in different experiments at the same potential. Furthermore, the average r_h varies about thirtyfold between 16 and 40 mV depolarization, while the average $\Delta\sigma^2/\overline{\sigma^2}$ increases only threefold. However, it is still possible that the effects of non-stationarities are significant for small depolarizations and become negligible only at higher depolarizations, where the low-frequency noise associated with inactivation becomes predominant. Therefore, we also have tried to obtain a theoretical estimate of the non-stationarity errors.

For an exact evaluation one requires information about the long-range correlations, associated with the slow drifts of our records. One must know the autocovariance function, $C(t, t+\tau)$, appearing in eqn. (3). Under the assumption already discussed, that Na channels have only one non-zero conductance level, the same kind of argument that leads to eqn. (8) (Conti & Wanke, 1975; Neher & Stevens, 1977) allows us to obtain, more generally:

$$C(t, t+\tau) = Ni^2p(t)\{\pi(\tau) - p(t+\tau)\}, \tag{12}$$

where $\pi(\tau)$ is the conditional probability that a Na channel is open at time τ if it was open at time zero. The time course of the open probability, $p(t)$, is directly measurable through $I(t)$ or through $\sigma^2(t)$:

$$I(t) = Nip(t) \tag{13a}$$

$$C(t, t) = \sigma^2(t) = Ni^2p(t)\{1\text{-}p(t)\} \tag{13b}$$

However, the transition probability $\pi(\tau)$ is not known, since values of τ are of the order of the duration of our samples. Let us consider a hypothetical Na channel in which a relatively fast activation-inactivation process (μ) is superimposed on an independent, slow inactivation (η). Then

$$p(t) = p_\mu p_\eta(t), \text{ and}$$

$$\pi(\tau) = \pi_\mu(\tau)\pi_\eta(\tau) = \{\pi_\mu(\tau) - p_\mu\}\pi_\eta(\tau) + p_\mu\pi_\eta(\tau) \tag{14}$$

$$\simeq \pi_\mu(\tau) - p_\mu + p_\mu\pi_\eta(\tau).$$

The μ process is already at equilibrium when our fluctuation measurements start ($t = 0$), while the η process has a relaxation time of the order of T. Although this case is not general, it can be used to estimate the order of magnitude of the possible systematic errors in the spectral points. If the slow inactivation is described by a single time constant, τ_η, then

$$p_\eta(t) = p_{\eta,\infty} + (p_{\eta,0} - p_{\eta,\infty})e^{-t/\tau\eta}, \tag{15}$$

$$\pi_\eta(\tau) = p_{\eta,\infty} + (1\text{-}p_{\eta,\infty})e^{-\tau/\tau\eta}, \tag{16}$$

and eqn. (12) becomes

$$C(t, t+\tau) = Ni^2 p_\eta(t)\{p_\mu[\pi_\mu(\tau)-p_\mu] + p^2{}_\mu[1-p_\eta(t)]e^{-\tau/\tau_\eta}\}. \quad (17)$$

Thus, the autocovariance of the fluctuations is the sum of two contributions associated one with the process that is in the steady state and the other with the slowly varying process. Inserting eqn. (17) into eqn. (3) and taking Fourier transforms to obtain power spectral densities allows one to evaluate the latter contribution for particular examples.

We give here the results of such evaluations for two cases corresponding to the largest non-stationarities observed. We assumed the spectrum of the steady-state process to be described by the HH scheme with $h_\infty \simeq 0{\cdot}12$ ($V = 16$ mV), and a slow inactivation producing a 40% decline of Na currents during the period T. For $\tau_\eta = T/2$, $p_{\eta,\infty} = 0{\cdot}28$ and $p_{\eta,0} = 0{\cdot}52$, we estimated that the first low-frequency point of our measured spectra would contain a contribution from the slow inactivation process of the order of 10% of that due to ordinary inactivation. For $\tau_\eta = T$, $p_{\eta,\infty} = 0{\cdot}22$ and $p_{\eta,0} = 0{\cdot}61$, that contribution would fall to about 3%. These errors should decrease quadratically with frequency. Thus, there is empirical and theoretical support to the conclusion that the spectral measurements are not significantly affected by the slow non-stationarities.

Analysis of power spectra

The spectra of Fig. 3 show that the Na current fluctuations contain a spectral component with a cut-off frequency in the range of 20–100 Hz, the frequency increasing with membrane depolarization. It is also seen that the relative amplitude of this component strongly increases with membrane potential. Independently of the particular kinetic scheme of Na channels that one selects, this component is expected to be present if the scheme adequately describes the inactivation of Na currents. Theory predicts (see, e.g. Colquhoun & Hawkes, 1977) that each genuine exponential component in the relaxation of the macroscopic current corresponds to a Lorentzian component in the fluctuation spectrum and vice versa.

For a quantitative evaluation we fitted spectra as in Fig. 3 with the function

$$s(f) = \frac{S(f)}{b\bar{\sigma}^2} = r_h s_h(f) + (1-r_h)s_m(f), \quad (18)$$

where $0 < r_h < 1$,

$$s_h(f) = L(f, \tau_h), \text{ and} \quad (19)$$

$$s_m(f) = \frac{1}{1-m_\infty^3} \sum_{j=1}^{3} \binom{3}{j} (1-m_\infty)^j m_\infty^{(3-j)} L(f, \tau_m/j). \quad (20)$$

The Lorentzian function is defined here as $L(f, \tau) = 4\tau/\{1+(2\pi f\tau)^2\}$. Eqn. (18) also defines how measured spectral densities $S(f)$ were normalized with respect to the corrected variance. The correction factor for the variance was

$$b = \left\{\int_0^{f_c} [r_h s_h(f) + (1-r_h)s_m(f)]\,df\right\}^{-1}, \quad (21)$$

where f_c is the cut-off frequency of our low-pass filter (5 kHz).

The terms $s_h(f)$ and $s_m(f)$ represent power spectra with unity variance. To the extent that the inactivation of transient Na currents is described by a single exponential, the identification of $s_h(f)$ with a simple Lorentzian according to eqn. (19) is independent of the model used to describe sodium channel kinetics. The use of eqn. (20) is also justified empirically: it describes reasonably well the shape of the spectrum at high frequencies. For a channel behaving exactly like the HH model, the value of r_h is (see eqn. (17) of Conti *et al.* 1976*a*):

$$r_h^{(HH)} = m_\infty^3(1-h_\infty)/(1-m_\infty^3 h_\infty). \tag{22}$$

Notice that although $r_h^{(HH)}$ is generally small, the low-frequency amplitude of the first component in eqn. (18) can become relatively large, since

$$\lim_{f\to 0} s_h(f) = 4\tau_h \gg 4\tau_m > \lim_{f\to 0} s_m(f).$$

In the fit of experimental spectra with eqns. (18)–(21), values of h_∞, $\tau_h = \tau_h''$ and m_∞ were fixed to those derived from the macroscopic currents on the same node (or, where not available from the same node, to the mean values of Table 1) and allowing r_h and τ_m to vary. The values of r_h and τ_m from these fits are given in Tables 5 and 4.

The values of τ_m obtained from the macroscopic currents (Table 1) are only roughly similar to the microscopic time constants in Table 4, revealing differences larger than the scatter among repeated measurements. The systematic deviations suggest that the HH model does not adequately represent the activation process. Even larger discrepancies were found in comparing empirical r_h values with $r_h^{(HH)}$ calculated from eqn. (22) (Table 5): the component of the fluctuation spectrum reflecting inactivation kinetics is systematically larger than predicted by the HH scheme. This result is illustrated in Fig. 4 showing a semilogarithmic plot of the $r_h^{(HH)}/r_h$ ratios versus membrane potential. The ratio is close to unity only for the largest depolarizations but becomes smaller at the small depolarizations. This result is independent of the exponent of m chosen to describe Na activation. If activation was described by m^a, with $a \neq 3$, $r_h^{(HH)}$ would be given by eqn. (22) with m_∞^3 substituted by m_∞^a. Since m_∞^a is empirically determined from the Na currents, it is invariant with a. Thus choosing another exponent form could not remove the discrepancies between the measured and the predicted r_h values: the HH model predicts too little variance for the slow fluctuation when the depolarization is small.

Comparison with predictions from other schemes

The values of r_h predicted by scheme (A), with $q' = q'' = 0$ and $q = 0{\cdot}5$, $q = 1$ or $q = 5$, were evaluated for the theoretical spectra. Those were computed as outlined by Colquhoun & Hawkes (1977), and with the parameters of Table 2. The results are given in Table 5 as $r_h^{(q=0{\cdot}5)}$, $r_h^{(q=1)}$ and $r_h^{(q=5)}$. In Fig. 5, their ratios to the experimental r_h values are plotted versus the membrane potential. The coupled schemes yield, at low depolarizations, ratios slightly closer to unity than the HH scheme, but tend to exceed the correct ratio of one at larger depolarizations.

We also compared directly the measured spectra with those computed numerically

TABLE 5. Relative variance of the slow fluctuations: empirical values versus model predictions

Node	V (mV)	r_h ($\times 10^{-3}$)	$r_h^{(HH)}$ ($\times 10^{-3}$)	$r_h^{(q=0.5)}$ ($\times 10^{-3}$)	$r_h^{(q=1)}$ ($\times 10^{-3}$)	$r_h^{(q=5)}$ ($\times 10^{-3}$)
4	16	25	—	—	—	—
8	16	22	4·8	7·7	6·6	7·4
9	16	12	3·4	7·2	5·8	6·4
13	16	17	6·8	13	12	12
Mean	16	19	5·0	9·3	8·1	8·6
4	24	77	—	—	—	—
5	24	130	—	—	—	—
6	24	84	—	—	—	—
11	24	67·5	31	42	37	37
12	24	70·5	21	27	28	27
Mean	24	85	26	34·5	32·5	32
3	32	150	—	—	—	—
8	32	220	130	200	180	180
10	32	360	180	260	230	230
13	32	260	210	380	340	330
Mean	32	250	173	280	250	247
6	40	400	—	—	—	—
9	40	360	310	560	450	510
12	40	350	450	670	650	780
Mean	40	370	380	615	550	645
10	48	560	600	900	800	900

r_h was found from the fit of spectra with eqn. (18). $r_h^{(HH)}$ was calculated from eqn. (22) and the parameters in Table 1. Values of $r_h^{(q=0.5)}$, $r_h^{(q=1)}$, and $r_h^{(q=5)}$ were obtained by numerical calculations of the spectral components for the coupled models (scheme (A) with $q' = q'' = 0$ and q as indicated) based on the parameters of Table 2.

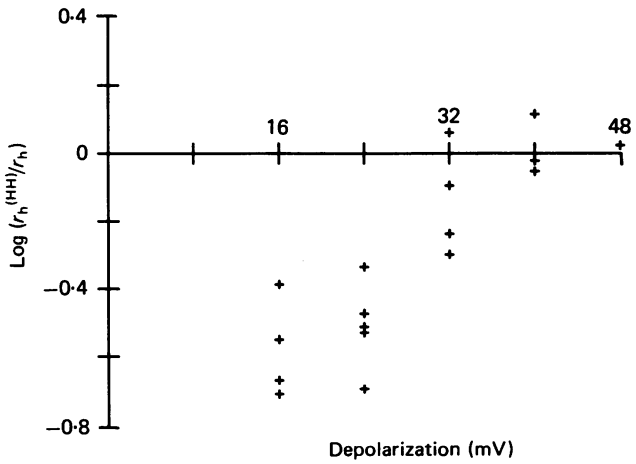

Fig. 4. Semilogarithmic plot of the ratio r_h^{HH}/r_h *vs.* depolarization. r_h is the measured relative contribution of inactivation noise to the total noise variance. r_h^{HH} is the theoretical expectation of r_h according to the HH scheme, calculated with the macroscopic parameters. The points are from the six nodes for which the full analysis of transient currents and fluctuations was performed (see Tables) and from four additional fibres.

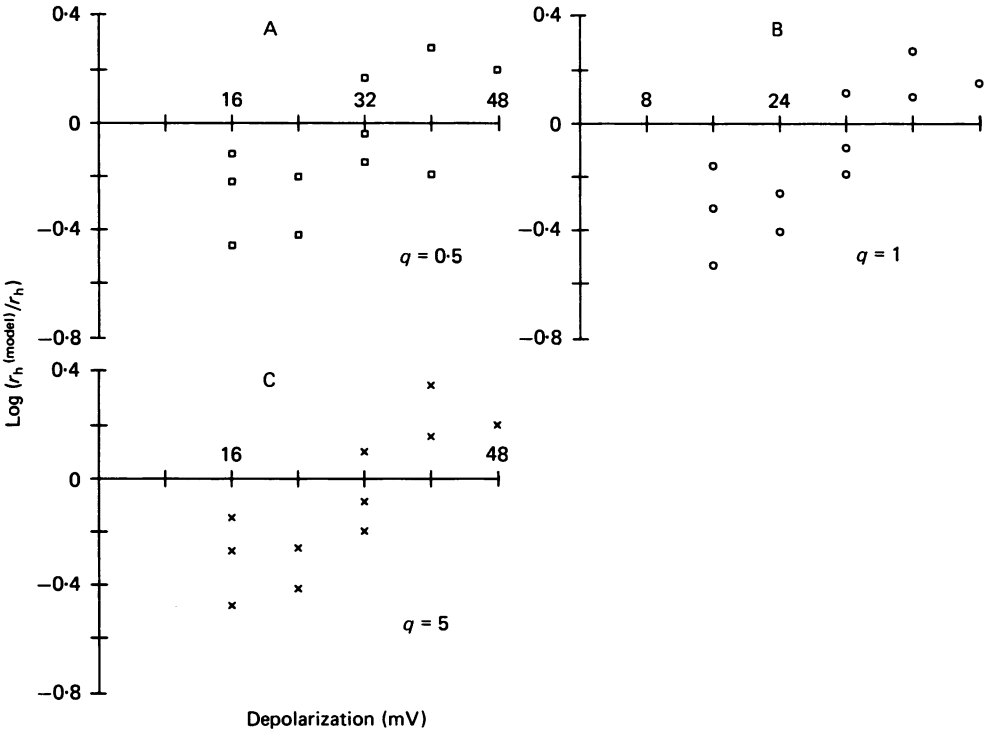

Fig. 5. Ratios $r_h^{(model)}/r_h$ for various coupled models versus depolarization. The models are represented by scheme (*A*) with $q' = q'' = 0$ and $q = 0{\cdot}5$ (*A*), $q = 1$ (*B*), or $q = 5$ (*C*). From same data as Fig. 4.

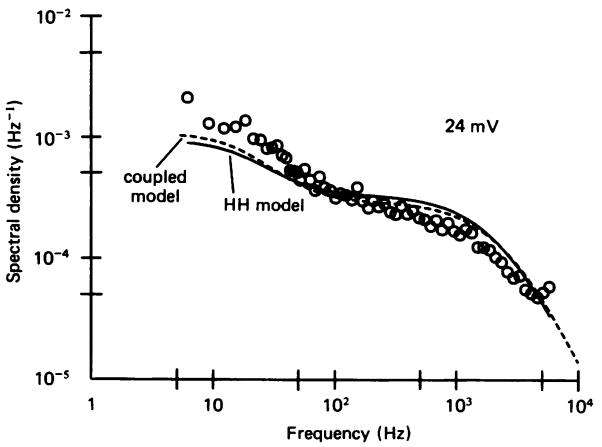

Fig. 6. Comparison of a measured fluctuation spectrum with the theoretical expectation of the Hodgkin-Huxley scheme (continuous line) or scheme (A) with $q = 0{\cdot}5$ (dashed line). The fits of the corresponding macroscopic currents are shown in Fig. 1 *B* and *E*. Depolarization 24 mV.

from the macroscopic parameters of the different models. An example is shown in Fig. 6 for a node in which fluctuation spectra were measured at 24 mV. The dashed curve gives the predicted spectrum according to scheme (A) with $q = 0{\cdot}5$ and for the same values of the parameters, α, β, κ and λ, used to obtain the fit of Fig. 1*E*. The continuous line gives the spectrum predicted from the HH scheme with the parameters used for the fit shown in Fig. 1 *B*. It is seen that the coupled scheme yields a slightly better agreement with the measured spectrum, but both schemes are evidently inadequate in reproducing the experimental points.

DISCUSSION

The experiments reveal low-frequency fluctuations in the nodal Na current that are attributable to the inactivation gating in Na channels. Thus, the fluctuation spectra (Fig. 3) are fairly flat at the low-frequency end (3 Hz) and begin to fall at frequencies close to those expected from the time constants of Na current inactivation. The slow fluctuations contribute little to the total fluctuation variance at 16 mV, but make up about one half of the variance at 48 mV (Table 5). This tendency is expected from the dual gating process of the Na channels: when channels are not inactivated during much of the time (16 mV), the rare and short activation events should dominate the fluctuations, while when non-inactivated channels are very likely to be activated (48 mV), the longer events due to the return from inactivation should emerge. On the other hand, we have carefully excluded that the low-frequency end of the experimental spectra has been artifactually enhanced by systematic processes: the trends in the membrane current have been eliminated by analyzing only the difference between each two subsequent records, and the possible errors due to a non-stationary, long-term inactivation process (Fig. 2) are shown to be negligible. The upper limit for a $1/f$ noise component given by Conti *et al.* (1976*a*) must now be moved downward; if such a component is present, it is too small for a reliable estimate at the frequencies above 3 Hz.

The single-channel conductance of 8·85 pS calculated from the total variance including the slow fluctuations is very similar to those found earlier, from stationary fluctuations attributable to the activation process (Conti *et al.* 1976*a*) or from non-stationary fluctuations during the transient Na current (Sigworth, 1977, 1979). Again, the apparent single-channel conductance is only weakly correlated to the degree of activation or inactivation at the voltage where fluctuations are measured. This confirms the previous conclusion that both gating processes switch the single-channel current between a large and a very small value (all-or-none gating). The criterion, however, does not indicate how many open or closed configurations the Na channel can assume, and the small variation of the apparent single-channel conductance (Table 4) would even be consistent with the existence of several open states that have slightly different conductances. The long-term inactivation process appears also to reduce the number of channels available for opening rather than the open-channel conductance.

We have used the fluctuation spectra for discriminating among several all-or-none gating models. Armstrong and Bezanilla (1977) have recently proposed a model in

which activation gates must be open for inactivation to occur. Then, the transition time constant ($1/(\lambda+\kappa)$) of the inactivation step must be smaller than the empirical inactivation time constant of the Na current (τ_h in the HH formalism). The authors suggested that the low-frequency fluctuations from such a channel would reveal the cut-off frequency $(\lambda+\kappa)/2\pi$ rather than $1/(2\pi\tau_h)$. Unfortunately, this simple test is not valid: the macroscopic current and the fluctuations, regardless of the specific model, are governed by the same time constants, each of which is in general a function of all transition rates in the model (Neher & Stevens, 1977). (The HH scheme is particular in having a time constant τ_h identical to that of the isolated inactivation step.) However, the components associated with those time constants have in general different weights in the macroscopic current and the fluctuation characteristics, and this was the basis for our test. We find that models with linked gating processes can predict the macroscopic currents (Fig. 1) and produce slightly larger, low-frequency fluctuations (Table 5) than the simplest microscopic version of the HH scheme, where activation and inactivation are mutually independent. Both kinds of schemes studied, however, are unable to predict the empirical contribution of the low-frequency fluctuations: at the small depolarizations, the low-frequency part of the fluctuations is found to be stronger in the experiments than in all of the models (Figs. 4–6).

Several aspects of our test need comment. First of all, the test shows that the otherwise important difference between linked and independent gating processes can be rather unimportant for the characteristics of the fluctuations. The main reason may be that in an inactivated channel there is no ionic current that could indicate whether activation transitions continue or not. We must conclude that fluctuation measurements are not a discriminating test of the ideas suggested by gating current immobilization experiments (Armstrong & Bezanilla, 1977; Nonner, 1980). The question is then, what causes the discrepancy between the measured size of the low-frequency fluctuations and the predictions of our models?

A reason may be that we used the wrong template (eqns. (18)–(20)) for dividing the spectrum into activation and inactivation components. As is already known (Chiu, 1977; Nonner, 1980), the inactivation of the nodal Na current is better described in terms of two exponential functions than by one. Two Lorentzian terms (with time constants differing by a factor of 4 (Nonner, 1980)) obviously would have fitted the low-frequency part of some of the spectra in Fig. 3 better than the single Lorentzian. However, if there are slow and fast transitions in the inactivation process, our method was likely to ascribe part of the fast inactivation fluctuations to activation and, thus, was unlikely to over-estimate the inactivation noise. Another possibility is that the template was inadequate for the activation noise. Indeed, values of τ_m from the fit of spectra and the fit of macroscopic currents (Tables 4, 1) were found to be significantly different, particularly at the large depolarizations. Paradoxically, this is the range of voltages where the analysis of the spectra and the model calculations gave similar fractions of low-frequency noise (Figs. 4, 5). The latter agreement could therefore be fortuitous. From a comparison of gating and Na currents, Armstrong & Gilly (1979) have recently proposed that activation may consist of several rapid steps followed by a slower step that opens the gate. If this model is applicable to frog Na channels, our analysis may have attributed part of the slower fluctuations of that activation

mechanism to inactivation, and we may have missed more of the rapid fluctuations than we considered when correcting for the limited band width (5 kHz) of the noise measurement. Both errors would have led to an overestimate of the relative inactivation variance. Finally, Na channels may have more than the single open state considered in the analysis. Transitions among several states with similar conductances would contribute only a small fluctuation variance, but the lifetimes of such states would be important in determining whether the random open-closed transitions occur frequently or less frequently. In squid axons, the decay of Na tail currents becomes slower when the length of the depolarizing pulse is increased, as if, during depolarization, Na channels passed through a first open state of short lifetime into a second open state of longer lifetime (Armstrong & Bezanilla, 1977). If this is true for nodal Na channels, fluctuation measurements during long depolarizations could yield larger activation time constants than those measured from the rise of the transient Na current, as it has been observed for the larger depolarizations (Tables 1, 4). With this modification alone, however, our models would hardly predict that there is so much low-frequency fluctuation at the small depolarizations (Table 5).

To summarize, our fluctuation measurements on Na currents are inconsistent with the simplest microscopic version of the Hodgkin–Huxley formalism. Modifying the model such that inactivation can occur only after partial or full activation yields fluctuation spectra closer to those observed, but the improvement is rather small. It seems necessary to study modifications on the activation process as well.

We thank Dr Bertil Hille for reading the manuscript, Dr Roberto Fioravanti for suggesting the subtraction procedure for eliminating systematic current drifts and Ms Lea Miller for invaluable technical help.

REFERENCES

ADELMAN, JR., W. J. & PALTI, Y. (1969). The effects of external potassium and long duration voltage conditioning on the amplitude of sodium currents in the giant axon of the squid, *Loligo pealei*, *J. gen. Physiol.* **54**, 589–606.

ARMSTRONG, C. M. & BEZANILLA, F. (1977). Inactivation of the sodium channel. II. Gating current experiments. *J. gen. Physiol.* **70**, 567–590.

ARMSTRONG, C. M. & GILLY, W. F. (1979). Fast and slow steps in the activation of Na channels. *J. gen. Physiol.* **74**, 691–711.

BEGENISICH, T. & STEVENS, C. F. (1975). How many conductance states do potassium channels have? *Biophys. J.* **15**, 843–846.

BEZANILLA, F. & ARMSTRONG, C. M. (1977). Inactivation of the sodium channel. I. Sodium current experiments. *J. gen. Physiol.* **70**, 549–566.

CHIU, S. Y. (1977). Inactivation of sodium channels: second order kinetics in myelinated nerve. *J. Physiol.* **273**, 573–596.

COLQUHOUN, D. & HAWKES, A. G. (1977). Relaxation and fluctuations of membrane currents that flow through drug-operated channels. *Proc. R. Soc.* B **199**, 231–262.

CONTI, F., DE FELICE, L. J. & WANKE, E. (1975). Potassium and sodium ion current noise in the membrane of the squid giant axon. *J. Physiol.* **248**, 45–82.

CONTI, F., HILLE, B., NEUMCKE, B., NONNER, W. & STÄMPFLI, R. (1976*a*). Measurement of the conductance of the sodium channel from current fluctuations at the node of Ranvier. *J. Physiol.* **262**, 699–727.

CONTI, F., HILLE, B., NEUMCKE, B., NONNER, W. & STÄMPFLI, R. (1976*b*). Conductance of the sodium channel in myelinated nerve fibres with modified sodium inactivation. *J. Physiol.* **262**, 729–742.

CONTI, F., NEUMCKE, B., NONNER, W. & STÄMPFLI, R. (1979). Low frequency fluctuations of Na current in myelinated nerve. *Pflügers Arch.* **379**, R40.

CONTI, F. & WANKE, E. (1975). Channel noise in nerve membranes and lipid bilayers. *Q. Rev. Biophys.* **8**, 451–506.

DODGE, F. A. & FRANKENHAEUSER, B. (1959). Sodium currents in the myelinated nerve fibre of *Xenopus laevis* investigated with the voltage clamp technique. *J. Physiol.* **148**, 188–200.

HODGKIN, A. L. & HUXLEY, A. F. (1952). A quantitative description of membrane current and its application to conduction and excitation in nerve. *J. Physiol.* **117**, 500–544.

LEE, Y. W. (1960). *Statistical Theory of Communication*. New York: J. Wiley and Sons.

NEHER, E. & STEVENS, C. F. (1977). Conductance fluctuations and ionic pores in membranes. *A. Rev. Biophys. Bioeng.* **6**, 345–381.

NONNER, W. (1969). A new voltage clamp method for Ranvier nodes. *Pflügers Arch.* **309**, 176–192.

NONNER, W. (1980). Relations between the inactivation of Na channels and the immobilisation of gating charge in frog myelinated nerve. *J. Physiol.* **299**, 573–603.

PEGANOV, E. M., KHODOROV, B. I., & SHISHKOVA, L. D. (1973). Slow sodium inactivation related to external potassium in the membrane of Ranvier's node. The role of external K. *Bull. exp. Biol. Med. U.S.S.R.* **25**, 15–19.

RICE, S. O. (1944). Mathematical analysis of random noise. *Bell System Techn. J.* **23**, 282–304. Also reprinted in *Selected Papers on Noise and Stochastic Processes*, ed. N. Wax. New York: Dover Publications, Inc., 1954.

SIGWORTH, F. J. (1977). Sodium channels in nerve apparently have two conductance states. *Nature, Lond.* **270**, 265–267.

SIGWORTH, F. J. (1979). Analysis of nonstationary sodium current fluctuations in frog myelinated nerve. Ph.D. Thesis, Yale University, New Haven, Connecticut.

SOONG, T. T. (1973). *Random Differential Equations in Science and Engineering*. New York: Academic Press.

STÄMPFLI, R. (1969). Dissection of single nerve fibres and measurements of membrane potential changes of Ranvier nodes by means of the double air gap method. In *Laboratory Techniques in Membrane Biophysics*, ed. H. Passow and R. Stämpfli. Berlin: Springer-Verlag.

VAN DEN BERG, R. J., DE GOEDE, J. & VERVEEN, A. A. (1975). Conductance fluctuations in Ranvier nodes. *Pflügers Arch.* **360**, 17–23.

VERVEEN, A. A. & DE FELICE, L. J. (1974). Membrane noise. *Prog. Biophys. molec. Biol.* **28**, 189–265.